Impact of the dipole contribution on the terahertz emission of air-based plasma induced by tightly focused femtosecond laser pulses

Alexander P. Shkurinov, Anton S. Sinko, Peter M. Solyankin, Alexander V. Borodin, Mikhail N. Esaulkov, Vladimir V. Annenkov, Igor A. Kotelnikov, Igor V. Timofeev, and Xi-Cheng Zhang

Phys. Rev. E **95**, 043209 — Published 20 April 2017

DOI: 10.1103/PhysRevE.95.043209

Impact of the Dipole Contribution into the Terahertz Emission of Air-Based Plasma in the Mode of Tight-focusing of the Femtosecond Laser Pulse

Alexander P. Shkurinov, Anton S. Sinko, and Peter M. Solyankin

Department of Physics and International Laser Center, Lomonosov Moscow State University, Leninskie Gory, Moscow, 119992, Russia

Alexander V. Borodin and Mikhail N. Esaulkov*

Institute on Laser and Information Technologies of the Russian Academy of Sciences - Branch of the FSRC "Crystallography and Photonics" RAS, Shatura, Moscow Region, Russia

Vladimir V. Annenkov, Igor A. Kotelnikov, and Igor V. Timofeev

Budker Institute of Nuclear Physics SB RAS and Novosibirsk State University, Novosibirsk, 630090, Russia

Xi-Cheng Zhang

The Institute of Optics, University of Rochester, Rochester, New York 14627-0186, USA.

(Dated: March 13, 2017)

Abstract

The present paper studies the generation mechanism of terahertz (THz) radiation from tightly focused femtosecond laser pulses in a gas medium. We measured the angular radiation pattern under different focusing conditions and observed that with the deepening of focus, the angular radiation pattern changes and optical-to-THz conversion efficiency increases. The analysis of the observed phenomena led to the assumption that the dipole radiation prevails in most cases despite the existing conception regarding the dominating role of the quadrupole mechanism of radiation. Based on these assumptions, the transient photocurrent theory of the phenomenon presented in this paper was developed by us and used for the numerical fit of the experimental data.

PACS numbers: 42.25.Bs; 42.65.Re; 42.65.Sf; 42.68.Ay; 52.38.Hb;

I. INTRODUCTION

Terahertz (THz) frequency range is one of the remaining scientific gaps in the electromagnetic spectrum with rich potential for scientific research [1]. The generation of THz radiation may occur in a gas medium when it is illuminated by intense femtosecond laser pulses. Initially, THz emission from a gas has always been associated with ionization of the gas, and the emission was thought to be exclusively driven by free electron currents [2, 3]. However, the THz radiation generation in air plasma is described nowadays with the assumption that there are two main physical mechanisms which actually take place under certain experimental conditions: four-wave rectification [4–6] and transient photocurrent [7–10] models. The manifestation and predominance of various mechanisms of THz generation depends on several factors: power density of the pump laser beam and whether "one-color" or "two-color" experimental scheme is used. In the "two-color" ap-

* esaulkov_mich@mail.ru

proach two ultrafast laser fields of fundamental and second harmonic frequencies interact in the gas medium, whereas in the "one-color" approach only one laser field at fundamental frequency is used for THz wave generation.

In the case of a comparatively weak laser pulse (below the ionizing threshold), the non-linear properties of the medium are determined by the neutral atoms of the medium [11], which leads to certain phenomena, including THz wave generation [6]. With the increase of the laser intensity, leading to the exceeding of gas ionization threshold, the second mechanism, which presupposes the radiation of free plasma electrons [12] in the shape of the transient photocurrent [7, 13, 14], becomes predominant. Assuming the additivity of several physical processes leading to radiation at the same frequency and quite incomplete ionization of gas, all these mechanisms work in laser plasma simultaneously. However, these contributions into the THz signal can be distinguished according to their spectral responses [15].

At the same time, the nonlinear optical signal can be presented in the form of the sum of dipole and quadrupole contributions [16, 17] if the nonlinear optical processes lead to the generation of the electromagnetic waves at the same frequency. Attempts to separate these waves date back to the early study of nonlinear optics [18, 19]. In THz non-linear optics the problem of separation of various contributions into the measurable signal is also actual, especially when they are of different origin [15].

In this paper, we study the influence of dipole and quadrupole currents on the THz radiation in the “one-color” experimental scheme. We carried out experiments on the generation of THz radiation under different focusing conditions, starting with a relatively long focal distances and gradually increasing the focusing depth until microplasma regime is reached.

In the paper we will use the term "filament" for the description of the interaction area with understanding that the term "filament" usually indicates a particular

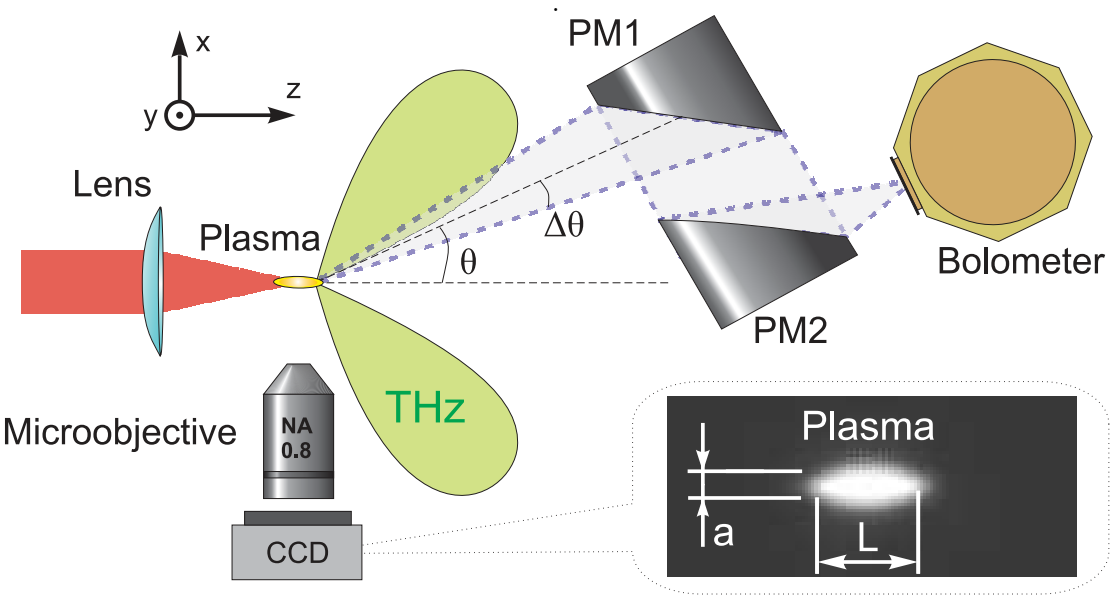

Figure 1. Schematic presentation of the experimental setup used to study the angular radiation pattern (top view): a laser beam is focused with a lens into ambient air. A pair of off-axis parabolic mirrors (PM1, PM2) positioned at angle θ from the optical beam axis collimates and refocuses the THz radiation into the window of Si bolometer. The angle θ can be continuously varied in the range $[-90°, 90°]$.

plasma structure where self-focusing is balanced by plasma diffraction. However, in the paper the length of the plasma is always defined by the geometrical focusing of the lens. However, we will use the term “filament”due to the evident unity of the main mechanisms of generation of THz radiation in our case and in the case of "extended filament".

II. EXPERIMENTAL SETUP

In order to justify our assumption, the experiment was carried out with the use of the setup shown in Fig. 1. The laser beam from Ti:Sapphire regenerative amplifier (Spectra Physics SpitFire Pro, 797 nm, 130 fs, pulse energy up to 1.5 mJ,

beam diameter up to 1 cm) was focused with one of the lenses into the ambient air. In order to change the length of the filament and its diameter we used a set of lenses having different focal distances: plano-convex lenses from fused silica with focal distances 100, 50, 40, 25, 7 mm and an aspherical acrylic lens CAY046 (Thorlabs. Inc) with effective focal distance 4.6 mm. A pair of Glan prisms and an iris aperture were used to manage and control the pulse energy in the interaction area and the laser beam diameter. The polarization of optical beam was kept linear and horizontal.

To estimate the dimensions of the filaments we analyzed the images of the plasma cloud appearing in the focal region. We collected images of the plasma fluorescence using a CoolSNAP Color (Roper Scientific) CCD camera with a microscope objective. Fluorescence bands of nitrogen and nitrogen ions (N_2 and N_2^+) which lie around 350-450 nm [20] contributed most to the observed filament image.

The collection system of THz radiation included a pair of off-axis parabolic mirrors (PM1 and PM2, diameter 50.6 mm, effective focal distance 101.2 mm) and a helium-cooled silicon bolometer (Infrared Laboratories General purpose 4.2 K bolometer). For studying the angular radiation pattern, the collection system was mounted on a rotation stage which could be rotated about the vertical axis which passes through the focal point of the lens. The detection angle θ between the optical beam axis and the first parabolic mirror PM1 could be varied in the range -90° to $+90^\circ$ where 0° corresponds to the propagation direction of the laser beam. The geometry of the setup does not allow us to study the THz radiation intensity in the backward direction, i.e. at the detection angles beyond $+90^\circ$ and -90°. The polarization of the THz radiation could be studied with help of a wire-grid THz polarizer placed between PM1 and PM2.

In this experiment, the multi-stage filtration system of THz radiation was utilized in order to prevent the influence of radiation of other spectral ranges. A

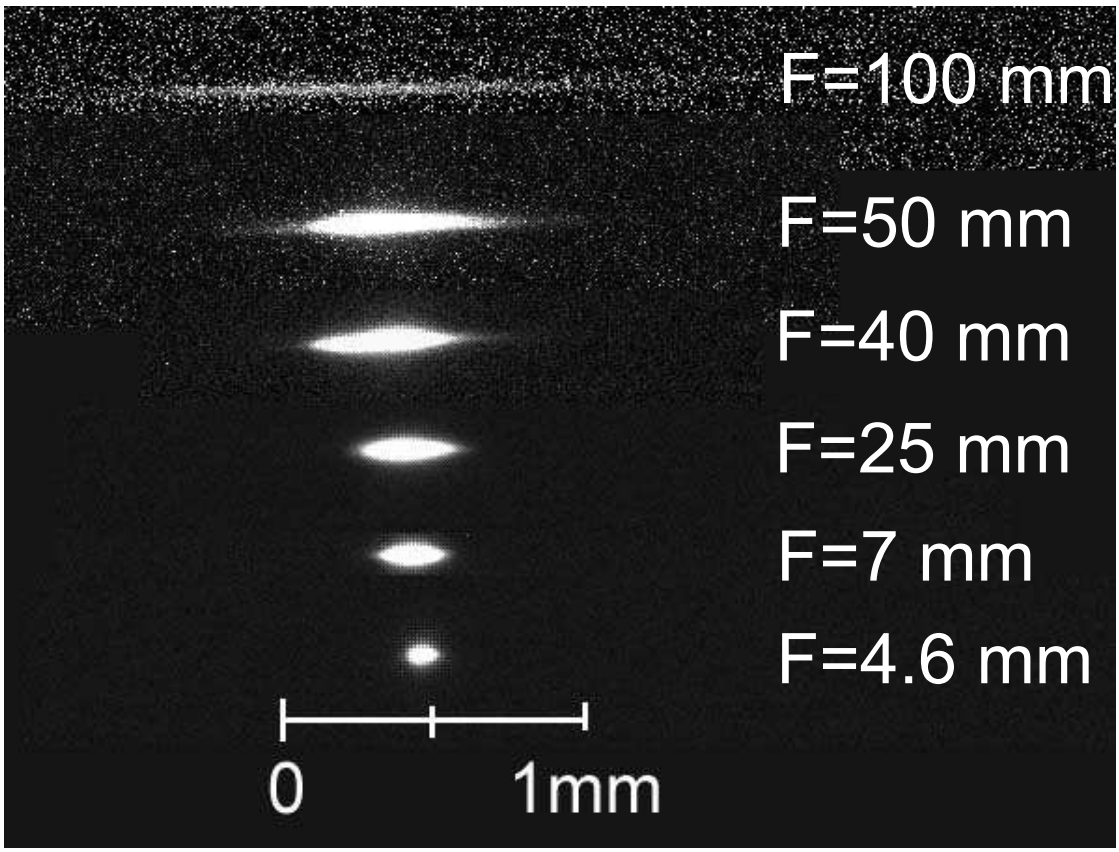

Figure 2. Side view CCD images of photo-induced plasma fluorescence taken at different focusing conditions. Measured length L and radii a of the filaments are indicated in Table I.

2.4 mm thick Teflon filter (transmission coefficient 0.85 over the THz spectral range of our study) was placed before the first parabolic mirror to scatter the pump radiation. Two 0.35 mm silicon wafers (10 Ohm·cm, boron doping, transmission coefficient of each wafer was 0.42 for normal incidence) were attached to the bolometer window. The input window of the bolometer was made from 1-mm thick HDPE (transmission coefficient 0.9). For complete separation of the THz signal, a 0.8 mm crystalline quartz filter with garnet powder was installed inside the bolometer and cooled to 4° K (transmission coefficient below 3 THz is 0.8, at higher frequencies the filter is non-transparent) which limits the range under study

to 0-3 THz. As we estimated from spectral measurements using a Michelson interferometer, most of the energy of THz radiation is concentrated in this spectral interval, which is also consistent with the results described in [21]. Total transmission coefficient of our filtering system in the range of 0.1-3 THz was approximately 0.1, while beyond this spectral range we estimate the transmission to be lower than 10^{-4}.

III. RESULTS OF THE MEASUREMENTS

For each lens with a different focal length we used a fixed optical beam aperture (7 mm) and maximum available pulse energy (700 μJ). The only exceptions were the acrylic lens with focal distance 4.6 mm (the aperture of the lens itself was 3.7 mm and the maximum pulse energy below the damage threshold was approximately 250 μJ) and the lens with focal distance 7 mm (maximum pulse energy was chosen 450 μJ to avoid optical damage). For all focusing conditions, we studied the dependence of intensity of THz radiation on the detection angle θ. Due to the fact that the first parabolic mirror has a limited aperture, it could collect only a part of the radiation emitted into large angles from the optical axis. This leads to the dependence of the radiation collection efficiency on the value of the emission angle, which has to be taken into consideration when processing experimental data. This procedure is described in the Sec. A of this paper.

The results of our measurements are shown in Fig. 3 with dots. It is clearly seen that for all focusing conditions, the in-plane angular radiation pattern contains two lobes of approximately equal intensity, which corresponds to the conical profile of the THz radiation. For all focusing conditions and linear polarization of the optical beam, we did not observe the dependence of the spatial profile of THz radiation on the direction of optical pulse polarization. Note that radiation distribution shown in Fig. 3 is not fully symmetric in θ. This effect was revealed only after numerical

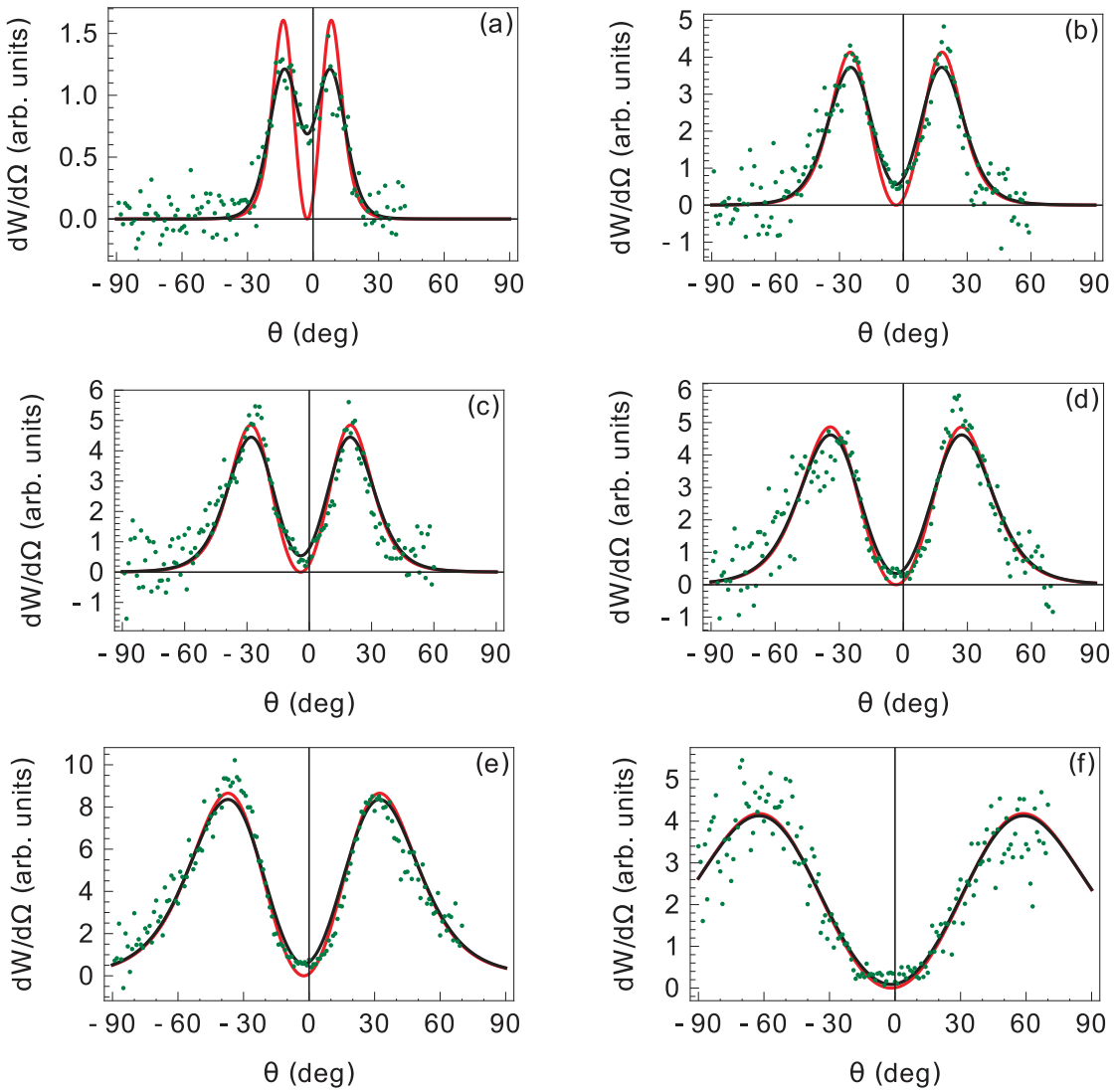

Figure 3. Measurements of angular distribution $\mathrm{d}W/\mathrm{d}\Omega$ of THz radiation for different focusing conditions (green dots), theoretical fit (red line) and theoretical fit corrected by instrumental function (black line); focal lengths F are indicated on the plots (see Table I for the parameters of the fit): (a) $F = 100\,\mathrm{mm}$, (b) $F = 50\,\mathrm{mm}$, (c) $F = 40\,\mathrm{mm}$, (d) $F = 25\,\mathrm{mm}$, (e) $F = 7\,\mathrm{mm}$, (f) $F = 4.6\,\mathrm{mm}$.

processing of the results of measurements. We suppose that this is because the central axis of our measuring system was slightly misaligned from the axis of the plasma channel.

To measure the polarization of the THz radiation, we set the detector angle θ equal to the direction of maximum of THz intensity (θ_{max}) and then rotated the THz polarizer placed between PM1 and PM2. In both lobes we observed maximum THz intensity when the polarizer orientation was horizontal. For vertical orientation of the polarizer, the THz intensity was from 10 to 50 times lower for longest and shortest focal distances of the lenses respectively. We observed the similar result when the polarization of the optical beam was changed to vertical linear. Our measurements agree with the earlier published studies [22] on the properties of radial polarization of the THz beam.

Due to the fact that the detector moves only in the horizontal plane and its aperture is limited, some amount of the THz radiation leaving the generator at large angles with respect to the horizontal plane cannot reach the bolometer since it will miss the aperture of the first parabolic mirror (PM1). Therefore we measured only part of the whole radiation pattern which was spread near the horizontal plane. That is why when we studied the radially polarized THz beam with conical spatial structure we saw only its part which was having linear horizontal polarization.

As we move towards shorter focal lengths of the lenses, the filament length becomes shorter (see Fig. 2), and the angle of maximum THz intensity $\theta_{\max}$ gets larger (see Fig. 3 and Fig. 4).

To compare the optical-to-THz conversion efficiency for different focusing conditions, we integrate the THz signal intensity over the emission angle from -90° to 90°. Here we take into account that the measured THz energy at large detection angles θ is only a part of the total energy emitted into that angle due to the finite aperture of the parabolic mirror, so that we need to multiply the raw data by a correction coefficient depending on the detection angle θ before the integration

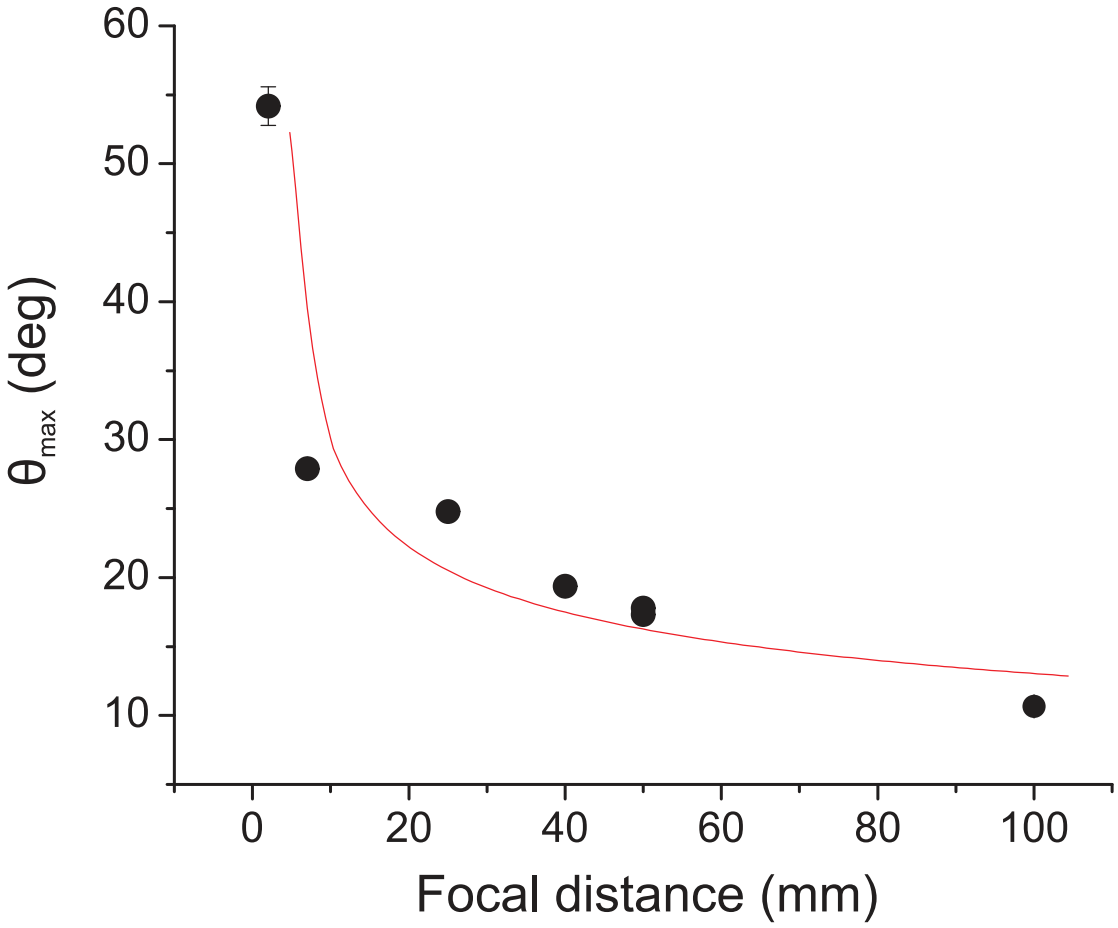

Figure 4. Angle $\theta_{\max}$ for which the maximum of the THz intensity is observed vs focal length

procedure. The procedure of calculating the correction coefficient is described in Sec. B. After that, we take as a figure-of-merit the integrated THz intensity divided by the optical pulse energy. Black circles in Figure 5 show the resulting conversion efficiency versus the focal distance of the lens. It is clearly seen that for the smallest focal distances, THz generation becomes more efficient. The smaller focusing radii F leads to increase in the peak laser intensity and plasma density [23] and sharpening of the field intensity gradients. As we see from our results, the efficiency of optical-to-terahertz energy conversion also increases, despite that the length and

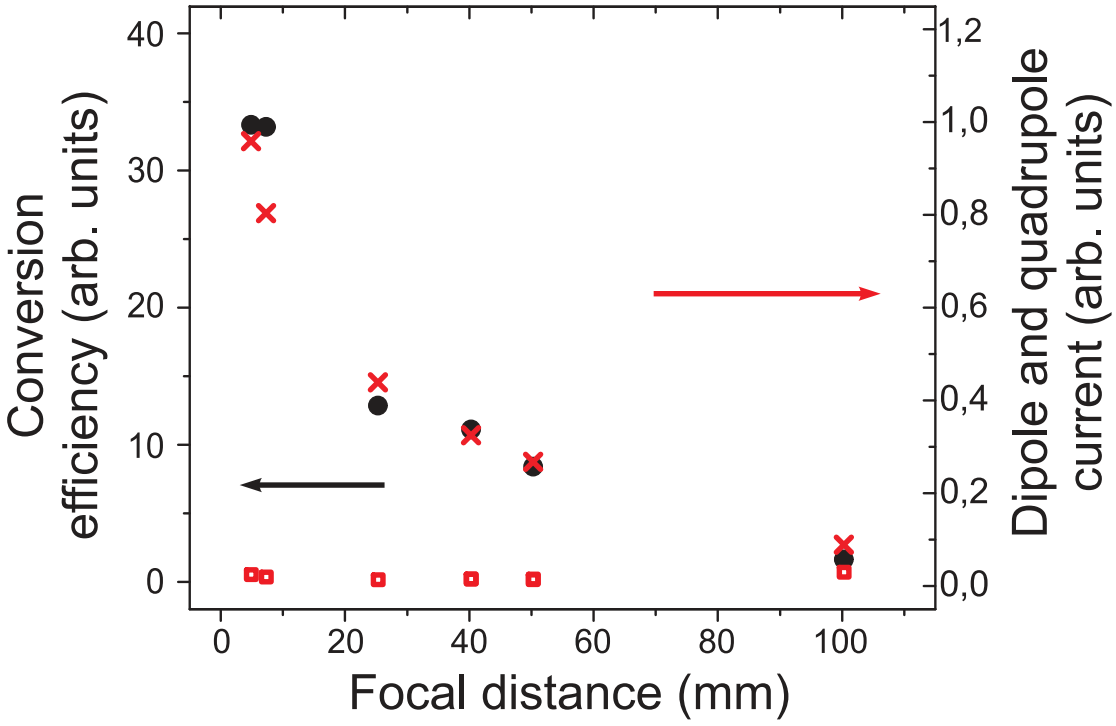

Figure 5. Black circles: efficiency of the optical-to-THz energy conversion versus focal length; red crosses: contribution of the dipole current to THz signal; red boxes: contribution of the quadrupole current to THz signal

the volume of the plasma channel decreases for deep focusing case. Therefore we conclude that the influence of decrease in the plasma dimensions plays inferior role in the optical-to THz conversion. Nevertheless, it becomes harder to collect all the emitted energy since the angle of the maximum emitted intensity θ_{max} can reach 55° (see Fig. 4).

IV. A MODEL OF THZ RADIATION

Previous phenomenological treatments of the problem of radiation from the plasma filament induced by a powerful laser pulse, such as [14, 24–27], did not take into consideration quantitative selection between the dipole and quadrupole

mechanisms of generation of the THz radiation. Here we consider contributions of both dipole and quadrupole currents inside the filament.

To extend the existing models we imagine that the current density $\mathbf{j} = \mathbf{j}(\mathbf{x}, t)$ induced in the filament by the pump laser pulse is already computed as a solution of the equations derived in [28, 29] or evaluated with the help of a PIC code. The Fourier transform $\mathbf{j}_\omega = \int_{-\infty}^{\infty} \mathbf{j}(\mathbf{x}, t)\, \mathrm{e}^{i\omega t}\, \mathrm{d}t$ of the current is related to the radiated magnetic field in the wave zone through the integral

$$\mathbf{B}_\omega(\mathbf{r}) = ik\mathbf{n} \times \frac{\mathrm{e}^{ikr}}{cr} \int \mathrm{d}^3x'\, \mathbf{j}_\omega(\mathbf{x}')\, \mathrm{e}^{-ik\mathbf{n}\cdot\mathbf{x}'}, \tag{1}$$

where $\mathbf{n} = \mathbf{r}/r$, and $k = \omega/c$ (see Eqs. (9.13) and (9.39) in [30]). The integral can be evaluated in an analytic form for two models of the current density profiles presented below. The difference between the two models will be clarified hereafter. Based on our PIC simulations (to be published elsewhere) and for the sake of simplicity we assume that the vector $\mathbf{j}$ has only the z-component and consider two profiles, namely:

$$j_z^{(1)}(x, y, z, t) = j_1 \frac{(z - ct)}{c\tau} \exp\left(-\frac{x^2 + y^2}{a^2} - \frac{(z - ct)^2}{c^2\tau^2} - \frac{z^2}{L^2}\right), \tag{2a}$$

$$j_z^{(2)}(x, y, z, t) = j_2 \frac{\partial}{\partial z}\left[(z - ct) \exp\left(-\frac{x^2 + y^2}{a^2} - \frac{(z - ct)^2}{c^2\tau^2} - \frac{z^2}{L^2}\right)\right]. \tag{2b}$$

The functions $j_z^{(1)}$ and $j_z^{(2)}$ simulate a pump laser pulse with the radius a and the length $c\tau$ propagating through a filament with the length L; the amplitudes j_1 and j_2 as well as the lengths L and a will be varied below when finding numerical fitting shown in Fig, 3. To justify this approach, we note that the authors of the recent paper [31] also assumed for the THz radiation to originate from the longitudinal electron current whereas the often discussed wake oscillations at the plasma frequency do not strongly contribute to the THz emission spectrum. The spacial profiles of the currents given by Eq. (2) roughly approximate those found in our preliminary numerical simulation.

The ponderomotive force of the pump laser pulse produces a longitudinal current structure, which propagates with approximately the speed of light [22, 31]. The interference of radiation from distinct points along the propagation axis leads to a conical emission. This mechanism of THz radiation is often referred to as transition-Cherenkov mechanism although the classic Cherenkov radiation requires the source moving at superluminal velocity, which is not the case under consideration.

The principal difference of the profile given by Eq. (2a) from Eq. (2b) is characterized by the value of $\int_{-\infty}^{\infty} j_z \, \mathrm{d}z$ which is nonzero in the case of dipolar type of charge distribution in the medium and zero in the case of higher orders of charge distribution. The condition $\int \mathbf{j}(\mathbf{x}, t) \, \mathrm{d}^3x = 0$, which holds for $j_z^{(2)}$ but not for $j_z^{(1)}$ means that the dipole moment of the system is permanently zero. Thus, $j_z^{(1)}$ is responsible for the dipole radiation whereas $j_z^{(2)}$ for the quadrupole one. It is also seen from the corresponding expressions for the magnetic field radiated by currents $j_z^{(1)}$ and $j_z^{(2)}$ and observed at the point with coordinates $\mathbf{r}$ at time t in the time domain. Due to axial symmetry, it has only the azimuthal α-component:

$$B_\alpha^{(1)} = \frac{\pi^{1/2}}{c^2 r} I_1 L \Delta\omega^3 \tau^2 \left(2\Delta\omega^2 t'^2 - 1\right) \mathrm{e}^{-\Delta\omega^2 t'^2} \sin(\theta), \tag{3a}$$

$$B_\alpha^{(2)} = \frac{\pi^{1/2}}{c^2 r} I_2 L \Delta\omega^4 \tau^3 \left(2\Delta\omega^2 t'^2 - 3\right) \Delta\omega t' \, \mathrm{e}^{-\Delta\omega^2 t'^2} \sin(2\theta) \tag{3b}$$

Here $I_1 = \pi a^2 j_1$ and $I_2 = \pi a^2 j_2$ are the total currents, $t' = t - r/c$ is the retarded time, and

$$\Delta\omega = \frac{c}{\sqrt{c^2\tau^2 + a^2 \sin^2\theta + L^2 \left(1 - \cos\theta\right)^2}} \tag{4}$$

is the spectral width of the radiation and θ is the angle between the filament axis and the direction to the radiation detector. In the case of a short filament ($L \to 0$) the dipole field (3a) varies with θ as $\sin(\theta)$ whereas the quadrupole field (3b) is proportional to $\sin(2\theta)$. Note that the frequency spectrum of the field is determined by the pump pulse duration τ, total length of the filament L and

the angle of observation θ. The duration of the radiated (THz) pulse is roughly evaluated as $T = 1/\Delta\omega$. In the forward direction ($\theta = 0$) it coincides with the pump pulse duration τ. It reaches maximal value $T \approx L/c$ for the pulse radiated at the right angle to the filament axis. The total energy

$$\frac{\mathrm{d}W}{\mathrm{d}\Omega} = r^2 \int_{-\infty}^{\infty} \frac{B^2}{4\pi}\,\mathrm{d}t$$

radiated into a given solid angle $\mathrm{d}\Omega = \sin\theta\,\mathrm{d}\theta\,\mathrm{d}\alpha$ can also be calculated in a closed form. As is seen from the result of the calculations

$$\frac{\mathrm{d}W}{\mathrm{d}\Omega} = \frac{3\pi^{3/2}}{16\sqrt{2}}\, c^2 L^2 \Delta\omega^5 \tau^4 \left[I_1^2 + 5 I_2^2 \Delta\omega^2 \tau^2 \cos^2\theta\right] \sin^2\theta, \tag{5}$$

the $j_z^{(2)}$ current does not interfere with $j_z^{(1)}$ (as there is no term proportional to $I_1 I_2$). We believe that the absence of the interference is not a typical case since an instant value of B^2 does contain the product $I_1 I_2$ but they disappear after integration over time.

Angular patterns predicted by Eq. (5) are shown in Fig. 6 for a selected set of parameters such that only either I_1 or I_2 is non-zero. The dipole and quadrupole angular patterns are visually different in the case of a short filament. If $L/c\tau \lesssim 0.4$ the quadrupole pattern has two visible backward lobes whereas the dipole pattern always has only two forward lobes. The backward lobes become too small in case of a long filament with $L/c\tau \gtrsim 1$. The width of the forward lobes and the angle θ_{max} at which the maximum radiation intensity is reached for quadrupole radiation is smaller than that for the dipole one at equal values of $L/c\tau$.

Moreover, the intensity of THz radiation resulting from the quadrupole current is zero in the direction orthogonal to the laser beam axis, i.e. at $\theta = 90°, -90°$ for any values of $L/c\tau$. The dipole and quadrupole angular patterns become actually indistinguishable if $L/c\tau \gtrsim 8$.

For the optical pulse with duration $\tau = 130\,\mathrm{fs}$ as in the reported experiment, the spacial length of the pump laser pulse is $c\tau \approx 39\,\mu\mathrm{m}$ which roughly leads to the

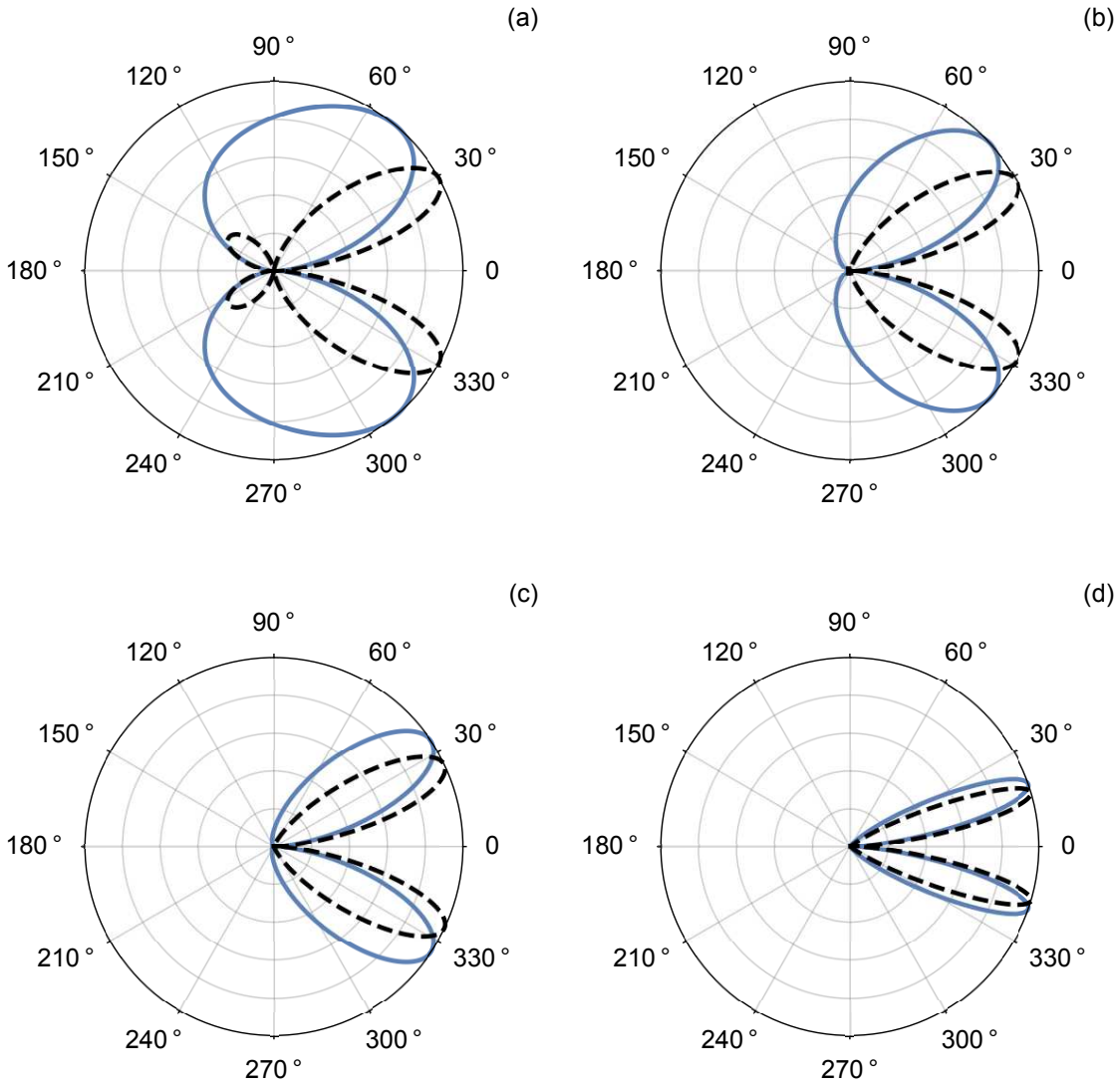

Figure 6. Angular patterns of $\mathrm{d}W/\mathrm{d}\Omega$ normalized over their maximums for $a = c\tau$ and various ratios $L/c\tau$: (a) 0.4, (b) 1, (c) 2, (d) 8; (blue) dipole radiation due to I_1, (black dashed) quadrupole radiation due to I_2.

experimentally measured values of the ratio $L/c\tau \gtrsim 1$ of the length of the plasma fluorescence pattern shown in Fig. 2 to the value of $c\tau$. As shown in Table I the experimental and fitted values of $L/c\tau$ coincide within the factor of 2−3 showing the same tendency as in the case when the focus length F varies.

	Experiment		Fit #1			Fit #2		
F (mm)	L	a	I_1	I_2	L	I_1	I_2	L
100	61.5	4.3	0.71	0.13	24.71	0.00	0.53	16.72
50	16.7	2.6	2.14	0.01	6.99	0.00	1.37	4.87
40	18.0	3.1	2.60	0.01	5.62	0.00	1.73	3.82
25	12.1	3.5	3.51	0.00	3.32	0.00	3.61	1.58
7	9.7	6.7	6.43	0.05	2.34	0.00	5.22	1.22
4.6	4.1	4.8	7.67	0.09	0.76	0.00	22.55	0.17

Table I. Experimental and fit parameters of the filaments; the values of L and a are normalized over the laser pulse length $c\tau$ which in our experimental conditions was equal to 39 μm .

For a large ratio $L/c\tau$ the opening angle of the radiation cone scales as $\theta_{\max} \approx \sqrt{c\tau/L}$ for both the dipole and quadrupole patterns. Returning to Eq. (4), one can see that $T \approx 2\tau$ for the THz radiation propagating at the angle $\theta_{\max}$.

V. NUMERICAL FIT

Equations (5) were used to fit experimental data as shown in Fig. 3. At first we tried to approximate the data with the function (5) by assuming both quadrupole and dipole nature of the emitting current, i.e. by varying I_1, I_2, L, and a. When computing numerical fits, we took into account the response function of our detection system as a 2D Gaussian profile with the width $\Delta\theta = 6^\circ$ as described in Sec. A.

The result is presented in Table I as Fit #1. It reveals significant domination of the dipole current even at large focus length F when the filament length L is so large that the dipole and quadrupole radiation are hardly distinguishable. As seen in Table. I, the quadrupole current I_2 is small as compared to the dipole current

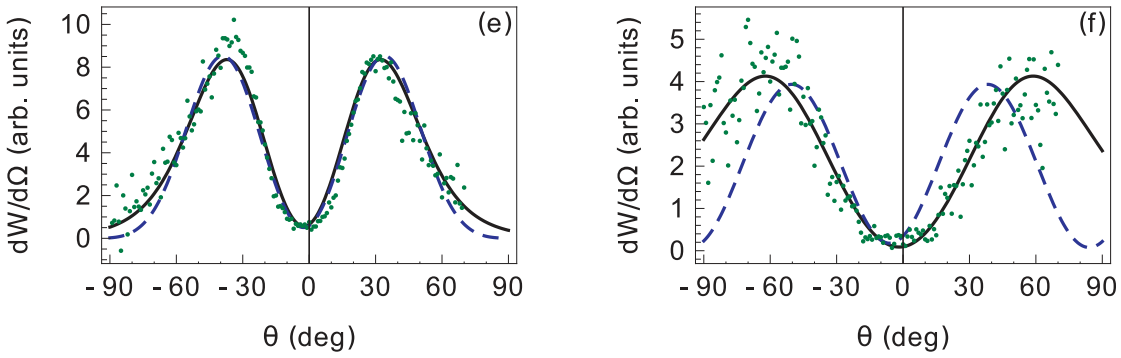

Figure 7. Comparison of the numerical fits: #1 (solid line) and #2 (dashed line).

I_1. We conclude therefore that

$$\frac{\mathrm{d}W}{\mathrm{d}\Omega} \approx \frac{3\pi^{3/2}}{16\sqrt{2}}\, c^2 L^2 \Delta\omega^5 \tau^4 I_1^2 \sin^2\theta. \tag{6}$$

We then repeated the fitting procedure with the dipole current forcibly set to zero. The result is presented in Table I as Fit #2. By comparing the residuals for the two fits we conclude that fit #1 is better for any F even though the plots for the fit #2 is visually indistinguishable at large F from the corresponding plots for fit #1 in Fig. 3. The most significant difference is observed at small F as shown in Fig. 7 for $F = 7\,\mathrm{mm}$ and $F = 4.6\,\mathrm{mm}$.

We also plot the results of the fits normalized to unity in the Figure 5 along with the energy conversion efficiency. As we see from the graph, the contribution of the dipole current increases as the focusing distance decreases while the quadrupole contribution is small and its value remains on approximately the same level for all focusing conditions.

As we see from the results of the fits, the computed dimensions of the THz emitter are smaller than the visible dimensions of the filament. This means that most of the THz radiation is generated in the thin part of the plasma where the plasma density is close to the critical value for THz radiation. The inner part of the plasma is not transparent for THz radiation, and the outer layers of plasma have

much lower electron density so that their contribution into the observed signal is also lower. Also, the dimensions of the plasma cloud, if measured using the CCD, are most likely overestimated due to expansion of the plasma after passing of the optical pulse. We observed the same phenomena in filaments formed in the gas cluster medium where the dimensions of the nonlinear medium emitting THz waves may be measured also by observing the X-ray radiation from the clusters [32].

VI. CONCLUSIONS

In order to clarify the nature of THz radiation which occurs in the case of deep focusing of laser radiation in "one-color" experimental scheme, we compared the contributions of dipole and quadrupole currents taking place in plasma. We discovered that the dominating contribution can be determined on the basis of the analysis of spatial distribution of THz radiation intensity. Besides, the radiation caused by quadrupole current under deep focusing leads to narrower peaks in the angular distribution of THz radiation intensity compared to the radiation caused by the dipole current. The quadruple photocurrent is also characterized by zero value of THz radiation intensity in the direction, orthogonal to the laser pulse propagation axis; and the presence of petals of the radiation propagation, which are directed backwards, are not characteristic for the dipole photocurrent. Moreover, the present paper is the pioneer in the development of the theoretical dependence of the measured duration and spectral width of THz pulse on the observation angle - detection angle θ (see Equation (4)). As we see from our experimental results and the theoretical fits, the spatial profile and the energy of the THz emission is mostly defined by the contribution of the longitudinal dipole current but not the quadrupole one for all focusing conditions under study. The part of the plasma cloud which contributes to the observed THz radiation is shorter

than the visible filament length measured with the help of a CCD camera. The efficiency of optical-to-THz energy conversion increases as well as the amount of the dipole contribution for the case of deep focusing of the laser radiation.

ACKNOWLEDGMENT

We appreciate useful comments on this work from Dr. Fabrizio Buccheri and Kang Liu. This work was supported the Russian Federation President Grant for Leading Scientific Schools (Grant No. NSh-9695.2016.2) and by Russian Foundation for Basic Research (Grants No. 15-32-20966, 15-32-20961, 14-22-01098 and partially Grant No. 16-32-60171).

Appendix A: Response function

We assume that a theory allows us to calculate the angular distribution of THz radiation in the form

$$\frac{\mathrm{d}W}{\mathrm{d}\Omega} = f(\theta), \tag{A1}$$

where $f(\theta)$ is given, e.g., by the RHS of Eq. (5). Then the angular distribution which takes into account the instrumenta responsel function $h(\theta, \theta')$ is determined by

$$\left(\frac{\mathrm{d}W}{\mathrm{d}\Omega}\right)_h = \int_0^\pi h(\theta, \theta')\, f(\theta')\, \mathrm{d}\theta'. \tag{A2}$$

To find $h(\theta, \theta')$, we take into account that the measured signal from the cone-shaped angular distribution is collected with the help of anaperture of the first parabolic mirror PM1. We consider here that each point of the detector parabolic mirror PM1 corresponds to a single point of a round "detector window" placed at the distance r (equal to focal distance of PM1). We write the Cartesian coordinates $\{x, y, z\}$ of an arbitrary point on the detector window via the spherical coordinates

$\{r, \alpha, \theta\}$ with the origin at the point of the laser focus:

$$\{x, y, z\} = \{r \sin\theta \cos\alpha, r \sin\theta \sin\alpha, r \cos\theta\}.$$

The square of the distance between two such points (on the detector window) with the coordinates $\{r, \alpha, \theta\}$ and $\{r, \alpha', \theta'\}$ is

$$l^2 = 2r^2 \left(1 + \cos\theta \cos\theta' - \sin\theta \sin\theta' \cos(\alpha - \alpha')\right),$$

so that

$$\left(\frac{\mathrm{d}W}{\mathrm{d}\Omega}\right)_h = \int_0^\pi \mathrm{d}\theta' \sin(\theta') \int_{-\pi}^{\pi} \mathrm{d}\alpha' h_2(\{\theta, \alpha\}, \{\theta', \alpha'\})\, f(\theta'), \tag{A3}$$

where h_2 is a two-dimensional instrumental response function. We approximate it by the Gaussian distribution

$$h_2(\{\theta, \alpha\}, \{\theta', \alpha'\}) = \frac{A}{\pi \Delta\theta^2} \exp\left[-\frac{l^2}{r^2 \Delta\theta^2}\right]. \tag{A4}$$

The integration over α' in Eq. (A3) can be done in a closed form. Comparing the result with Eq. (A2) we find the one-dimensional instrumental response function:

$$h(\theta, \theta') = \frac{2A \sin(\theta')}{\Delta\theta^2}\, \mathrm{e}^{-2(1-\cos\theta\cos\theta')/\Delta\theta^2}\, \mathrm{I}_0\left(\frac{2 \sin\theta \sin\theta'}{\Delta\theta^2}\right), \tag{A5}$$

where I_0 denotes the Bessel function. In the case of $2\sin\theta \sin\theta' \gg \Delta\theta^2$, this expression transforms to

$$h(\theta, \theta') = \frac{A\sqrt{\sin\theta'}}{\sqrt{\pi}\Delta\theta\sqrt{\sin\theta}}\, \mathrm{e}^{-4\sin^2\left(\frac{\theta-\theta'}{2}\right)/\Delta\theta^2}.$$

The constant A is determined from the condition

$$\int_0^\pi \mathrm{d}\theta' h(\theta, \theta') = 1$$

and is equal to

$$A = \frac{1}{1 - \mathrm{e}^{-4/\Delta\theta^2}} \approx 1.$$

We took $\Delta\theta = 6°$, which provides the best numerical fit to the angular diagrams in case of long filaments.

Appendix B: Correction multiplier

Let R be effective focusing distance of the first parabolic mirror. The effective aperture of the first parabolic mirror in the detection system (PM1) can be represented as a circle with radius R_{parab} moving along a circle with radius R in the horizontal plane and collecting radiation fro, a part of the "detection sphere" with radius R which can move in the horizontal plane when we rotate the detection sysem (see Fig.). Let us assume that in the focal point of the parabolic mirror we have a source of THz radiation emitting in a narrow cone with cone angle θ and very narrow angular width ($\Delta\theta \approx 0$) and a homogeneous distribution over the azimuth angle α. Emission from this source crosses the "detection sphere" with radius R along a circle with radius $R\sin\theta$. It is clear that if $R\sin\theta > R_{parab}$, part of the emitted radiation will miss the detector at any orientation θ_{detect} of the detector (in the Fig. 8, only the radiation shown by the dashed lines can be collected by the detector). In order to calculate the value of the correction coefficient by which the obtained signal should be multiplied in order to compare the energy efficiency of THz generation, we need to find the ratio of the length of the whole circle along which the THz radiation crosses the "detection sphere" ($2\pi R\sin\theta$) and by the length of its part that gets into the dashed area of the sphere. In the case of wide THz direction cone, when $R\sin\theta > R_{parab}$, the aperture of the detector positioned at the angle θ collects only part of the emitted energy. For the narrow cone of THz radiation, when $R\sin\theta < R_{parab}$, the detector collects all the emitted energy and therefore the correction multiplier equals 1. The values of the correction coefficient as a function of the emission angle θ for the sizes and focusing distance of the parabolic mirror used in the experiment are given in the Fig. 8 with the the scheme clarifying the idea.

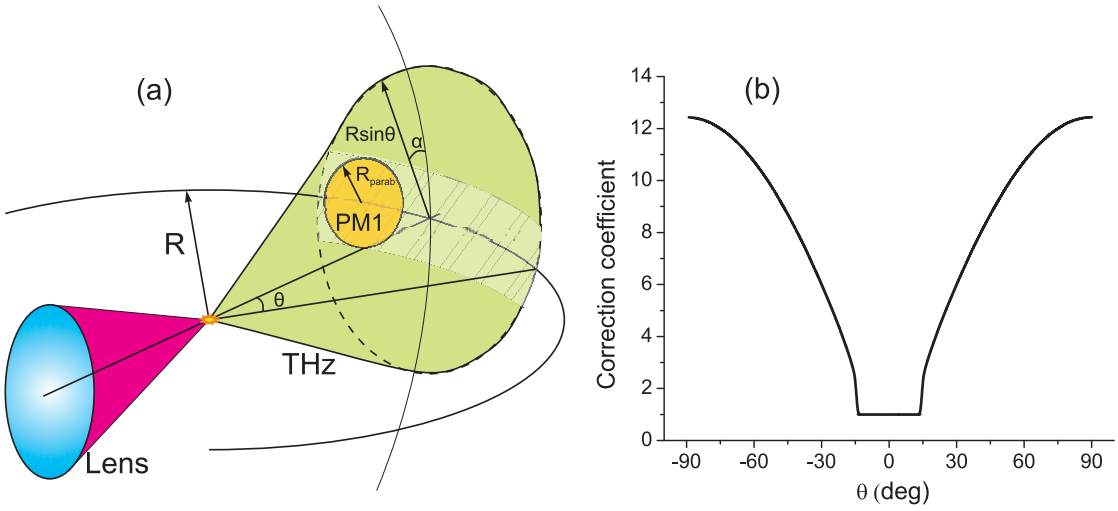

Figure 8. (a) Scheme showing the decrease in efficiency of THz radiation collection for wide emission cones. (b) Values of the correction coefficient for the used experimental parameters

[1] X.-C. Zhang, A. Shkurinov, and Y. Zhang, Nature Photonics **11**, 1 (2017).

[2] G. Askar'yan, JETP **15**, 943 (1962).

[3] H. Hamster, A. Sullivan, S. Gordon, W. White, and R. W. Falcone, Phys. Rev. Lett. **71**, 2725 (1993).

[4] M. Kreß, T. Löffler, M. D. Thomson, R. Dörner, H. Gimpel, K. Zrost, T. Ergler, R. Moshammer, U. Morgner, J. Ullrich, and H. G. Roskos, Optics Letters **29**, 1120 (2004).

[5] J. Dai, X. Xie, and X.-C. Zhang, Physical Review Letters **97**, 103903 (2006).

[6] D. J. Cook and R. M. Hochstrasser, Optics Letters **25**, 1210 (2000).

[7] K. Y. Kim, J. H. Glownia, A. J. Taylor, and G. Rodriguez, Opt. Express **15**, 4577 (2007).

[8] I. Babushkin, W. Kuehn, C. Köhler, S. Skupin, L. Bergé, K. Reimann, M. Woerner, J. Herrmann, and T. Elsaesser, Phys. Rev. Lett. **105**, 053903 (2010).

[9] V. A. Andreeva, O. G. Kosareva, N. A. Panov, D. E. Shipilo, P. M. Solyankin, M. N. Esaulkov, P. González de Alaiza Martínez, A. P. Shkurinov, V. A. Makarov, L. Bergé, and S. L. Chin, Phys. Rev. Lett. **116**, 063902 (2016).

[10] M. Clerici, M. Peccianti, B. E. Schmidt, L. Caspani, M. Shalaby, M. Giguère, A. Lotti, A. Couairon, F. Légaré, T. Ozaki, D. Faccio, and R. Morandotti, Phys. Rev. Lett. **110**, 253901 (2013).

[11] R. W. Boyd, *Nonlinear Optics*, second edition ed. (Academic Press, London, 1992).

[12] H. Hamster, A. Sullivan, S. Gordon, and R. W. Falcone, Phys. Rev. E **49**, 671 (1994).

[13] C.-C. Cheng, E. M. Wright, and J. V. Moloney, PRL **87**, 213001 (2001).

[14] A. V. Balakin, A. V. Borodin, I. A. Kotelnikov, and A. P. Shkurinov, J. Opt. Soc. Am. B **27**, 16 (2010).

[15] A. V. Borodin, N. A. Panov, O. G. Kosareva, V. A. Andreeva, M. N. Esaulkov, V. A. Makarov, A. P. Shkurinov, S. L. Chin, and X.-C. Zhang, Opt. Lett. **38**, 1906 (2013).

[16] N. I. Koroteev, Soviet Physics Uspekhi **30**, 628 (1987).

[17] A. P. Shkurinov, A. V. Dubrovskii, and N. I. Koroteevev, Phys. Rev. Lett. **70**, 1085 (1993).

[18] N. Bloembergen, R. K. Chang, S. S. Jha, and C. H. Lee, Phys. Rev. **174**, 813 (1968).

[19] E. Adler, Phys. Rev. **134**, A728 (1964).

[20] A. Talebpour, M. Abdel-Fattah, A. Bandrauk, and S. Chin, Laser Physics **11**, 68 (2001).

[21] F. Buccheri and X.-C. Zhang, Optica **2**, 366 (2015).

[22] C. D. Amico, A. Houard, S. Akturk, Y. Liu, J. L. Bloas, M. Franco, B. Prade, A. Couairon, V. T. Tikhonchuk, and A. Mysyrowicz, New Journal of Physics **10**,

013015 (2008).

[23] F. Théberge, W. Liu, P. T. Simard, A. Becker, and S. L. Chin, Phys. Rev. E **74**, 036406 (2006).

[24] J. Zheng, C. X. Yu, Z. J. Zheng, and K. A. Tanaka, Phys. Plasmas **12**, 093105 (2005).

[25] C. D'Amico, A. Houard, M. Franco, B. Prade, A. Mysyrowicz, A. Couairon, and V. T. Tikhonchuk, Phys. Rev. Lett. **98**, 235002 (2007).

[26] N. A. Panov, O. G. Kosareva, V. A. Andreeva, A. B. Savel'ev, D. S. Uryupina, R. V. Volkov, V. A. Makarov, and A. P. Shkurinov, JETP Letters **93**, 638 (2011).

[27] F. Jahangiri, M. Hashida, S. Tokita, T. Nagashima, M. Hangyo, and S. Sakabe, Applied Physics Letters **102**, 191106 (2013), http://dx.doi.org/10.1063/1.4804582.

[28] L. M. Gorbunov, P. Mora, and T. M. Antonsen, Physics of Plasmas **4**, 4358 (1997).

[29] H.-C. Wu, J. Meyer-ter Vehn, H. Ruhl, and Z.-M. Sheng, Phys. Rev. E **83**, 036407 (2011).

[30] J. D. Jackson, *Classical Electrodynamics*, 3rd ed. (John Wiley & Sons, Inc., 1999).

[31] I. Thiele, R. Nuter, B. Bousquet, V. Tikhonchuk, S. Skupin, X. Davoine, L. Gremillet, and L. Bergé, Phys. Rev. E **94**, 063202 (2016).

[32] A. V. Balakin, M. S. Dzhidzhoev, V. M. Gordienko, M. N. Esaulkov, I. A. Zhvaniya, K. A. Ivanov, I. A. Kotelnikov, N. A. Kuzechkin, I. A. Ozheredov, V. Y. Panchenko, A. B. Savel'ev, M. B. Smirnov, P. M. Solyankin, and A. P. Shkurinov, IEEE Transactions on Terahertz Science and Technology **7**, 70 (2017).